Journal of Constructional Steel Research 154 (2019) 123–133

Contents lists available at ScienceDirect

Journal of Constructional Steel Research

Seismic performance evaluation and improvement of ultra-high voltage wall bushing-valve hall system

Chang He, Qiang Xie, Zhenyu Yang, Songtao Xue *

College of Civil Engineering, Tongji University, China

ARTICLE INFO

Article history:
Received 19 June 2018
Received in revised form 15 November 2018
Accepted 17 November 2018
Available online xxxx

Keywords:
UHV
Wall bushing
Valve hall
Seismic performance improvement
Seismic interaction

ABSTRACT

To evaluate and improve the seismic performance of a ±800 kV ultra-high voltage (UHV) wall bushing-valve hall system, a finite element model of the system was established. Sixteen different earthquake ground motions were adopted in the analysis, and the critical seismic responses of the system were obtained. Moreover, a vibration theoretical model of the UHV wall bushing-valve hall system was established, and an investigation was conducted on the influence of different vibration components on the wall bushing seismic responses. The results indicate that the valve hall has an amplification effect on the seismic responses of the wall bushing and the vibration of the gable wall has a remarkable influence on the responses of the wall bushing. Two retrofitting measures were carried out on the valve hall to reduce the seismic responses of the wall bushing. It is concluded that increasing the stiffness of the gable wall could improve the seismic performance of the UHV wall bushing-valve hall system.

1. Introduction

Substations are critical nodes in the electrical lifeline system and vulnerable to earthquakes [1]. The failure of any substation may lead to power interruption and make it difficult in disaster relief and rebuilding. In past decades, earthquakes destroyed many substations and electric facilities. In the 1994 Northridge Earthquake (in and around Los Angeles, CA, USA), the seismic failure of the electric facilities in substations interrupted the power supply [2]. In 2007, a 500 kV porcelain transformer bushing was set on fire in the Niigata-Chuetsu Oki Earthquake in Japan and led to the outage of a nuclear power plant [3]. The 2008 Wenchuan Earthquake in Sichuan, China destroyed many insulators and bushings, which were always fractured at their base cross sections [4]. Additionally, the 2011 Tohoku Region Pacific Offshore Earthquake erupted with a magnitude of Mw 9.0, fracturing a total of 621 electric insulators, including many high voltage bushings [5]. Other notable earthquakes occurred in New Zealand in 2010 and 2011, which destroyed many electric facilities in substations [6].

Increasing the voltage could reduce the line loss in power transmission systems. In fact, the ultra-high voltage (UHV) direct current (DC) power transmission technology was developed to meet the needs of long-distance power transmission in China [7,8]. A UHV converter substation is defined as the substation adopted in a DC project where the design voltage is equal to or higher than ±800 kV. A wall bushing is indispensable in the converter substation for connecting the thyristor valves in the valve hall (indoors) and the post insulators in the DC yard (outdoors). Just as the name implies, the wall bushing is installed on the gable wall of a valve hall to keep the electric clearance between conductors and walls (Fig. 1).

Like the wall bushing mounted on the gable wall of the valve hall, many bushings and insulators are installed on supporting structure, e.g., transformer bushings mounted on turrets, surge arresters and post insulators mounted on steel frames. Recent studies have verified that a good seismic performance of bushings installed on a rigid base in a laboratory does not correspond well with the high vulnerability observed in the field during earthquakes. The experiments also imply that the interaction between bushings and supporting structures has an influence on the seismic performance of the equipment [9,10]. Further investigation revealed that the vibration of the turrets of a power transformer amplifies the seismic responses of transformer bushings and the amplification effect is one of the main reasons for the seismic failure of transformer bushings [11]. To suppress the amplification effect, Koliou et al. added flexural stiffeners on the cover plate of the transformer tank numerically and experimentally, and the amplification factors were reduced [10,12]. This phenomenon indicates that the amplification effect could be reduced by changing the supporting structural dynamic properties. In terms of pillar apparatus, the dynamic amplification effect of supporting structures has been investigated by researches. A theoretical model of the electric equipment-supporting structure has been established [13]. The stiffness ratio and mass ratio of equipment and the support structure on the dynamic amplification effect was studied [13]. For tests, Günay and Mosalam found that the insulators of the

* Corresponding author at: College of Civil Engineering, Tongji University, Siping Road 1239, Shanghai 200092, China.
E-mail address: xue@tongji.edu.cn (S. Xue).

https://doi.org/10.1016/j.jcsr.2018.11.016
0143-974X/

Fig. 1. ±800 kV UHV wall bushing mounted on a gable wall.

disconnect switch experienced the maximum responses when the fundamental frequencies of the insulators and the supporting structure were similar, which means that enlarging the fundamental frequency difference between the electric equipment and supporting frame could reduce the interaction between the two components [14]. Li et al. tested the dynamic amplification effect of the supporting frame of a 1000 kV UHV surge arrester and developed a structural design procedure for selecting the suitable supporting frame to minimize the amplification effect [15]. Whitaker et al. conducted a shaking table test on a 230 kV disconnect switch and carried out finite element (FE) analyses on the disconnect switch with different supporting frames. The influence of different supporting frames on the seismic responses of the disconnect switch was evaluated [16]. As for the seismic performance of the wall bushing, Xie et al. carried out shaking table tests on a full size UHV polymer wall bushing and found that the strength of the wall bushing does not satisfy the required relevant standards [17,18]. In the test, the bushing was mounted on a steel supporting frame, and the type of the wall bushing was same as the bushing in this paper. The fundamental frequency of the steel supporting frame was 44 Hz and could be seen as a rigid body. An amplification factor of 2 was adopted for the input earthquake ground motions to simulate the amplification effects of the valve hall [17].

However, few studies have been published on the interaction between the wall bushing and the valve hall; thus, the authors determined to fill some information gaps by evaluating the amplification effect of the valve hall. In the IEEE 693 standard and the GB 50260 standard, an amplification factor of 2.0 was adopted to evaluate the seismic performance of the transformer bushing mounted on a rigid base [18,19]. However, both the IEEE 693 and GB 50260 standards still lack stipulations about the interaction in the valve hall-wall bushing system [18,19].

Fig. 2 shows the dimensions of a type of 150 kV, 400 kV and 800 kV wall bushings. In addition, the lengths, masses, diameters, thicknesses and the fundamental frequencies of the wall bushings in three different levels of voltage are listed in Table 1. According to Fig. 2 and Table 1, as the voltage increases, the UHV wall bushing is longer, heavier than its counterparts using a lower voltage. The different responses to voltage increases makes the UHV wall bushing more vulnerable in earthquakes. Considering the importance of the UHV wall bushing, it is necessary to study the seismic performance of the wall bushing-valve hall system and the interaction between the wall bushing and the valve hall.

The purpose of this paper is to evaluate the seismic performance of the UHV wall bushing-valve hall system and to investigate the dynamic interaction between the wall bushing and the valve hall. An FE model, and a theoretical model of the UHV wall bushing-valve hall system

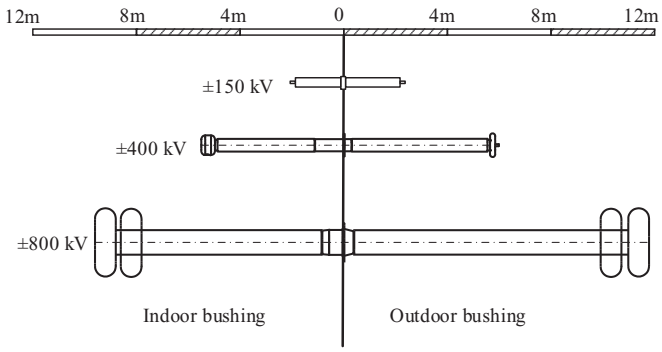

Fig. 2. Schematic diagram of the wall bushings at different voltage levels.

was established and analyzed. After that, two retrofitting measures for improving the seismic performance of the system were put forward and verified.

2. UHV wall bushing-valve hall system

2.1. Structure of valve hall

The length, width and height of a ±800 kV UHV valve hall, a steel structure used in many complete DC projects, are 86 m, 36 m and 31.6 m, respectively (Fig. 3). Distances of columns in the gable wall range from 5.4 m to 9 m. The columns GZ1 and GZ2 are wide flange H shaped member, with dimensions 900 × 600 × 20 × 28 and 700 × 500 × 16 × 25, respectively. The cross sections of the square tubes used for the beams between the columns are 200 × 200 × 8. Additionally, braces with cross section in wide flange H shape of 250 × 250 × 12 × 12 are placed between the columns and beams. The schematic diagrams of the steel valve hall are shown in Fig. 3. The shapes and dimensions of the cross sections of the beams, columns and braces of the valve hall are shown in Fig. 4. The wall bushing is mounted on the frame shown in the circle in Fig. 3(b). The beams, columns and braces of the frame are square tubes with dimensions of 400 × 400 × 13 (□400), 350 × 350 × 12.5 (□350) and 100 × 100 × 6 (□100), respectively.

2.2. UHV wall bushing

The insulators of the wall bushing are made from polymer material, a composite material widely used in electric facilities for insulation and structural elements. The wall bushing contains an indoor bushing, an outdoor bushing and a metal connection unit between the two polymer bushings to mount the equipment on the gable wall (Fig. 5). The indoor and outdoor bushings join the connection unit by flange. An aluminum conductor passing through the wall bushing transmits the electric current from the indoor terminal to the outdoor terminal. A resin-impregnated paper capacitor packet is wrapped around the central conductor to keep the stability of the electromagnetic field and to guarantee the effectiveness of the inner insulation of the wall bushing. Silicon rubber sheds around the external surfaces of the insulators are used

Table 1
Structural parameters of the wall bushing in different voltage.

Voltage (kV)	150	400	800
Length of indoor bushing (mm)	1460	3870	8100
Length of outdoor bushing (mm)	1860	5760	10,100
Length of mental connection unit (mm)	1020	1520	2000
Mass (kg)	675	1950	11,450
Outer Diameter (mm)	300	408	770
Thickness (mm)	8	18	25
Fundamental frequency (Hz)	25.3	7.32	1.51

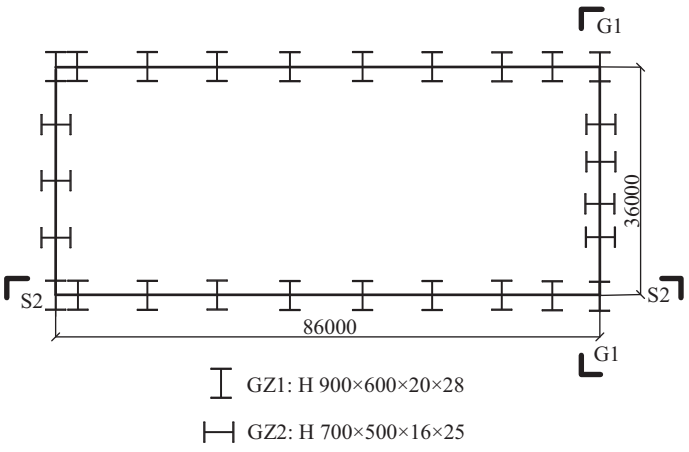

(a) Horizontal section of the valve hall

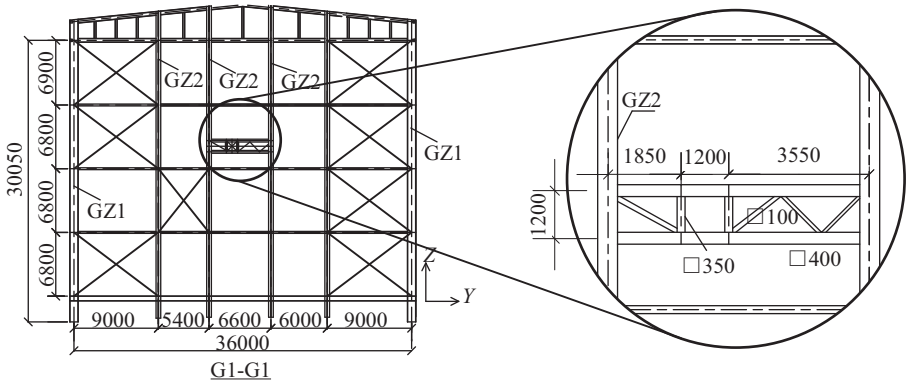

(b) Front view (gable wall) of the valve hall

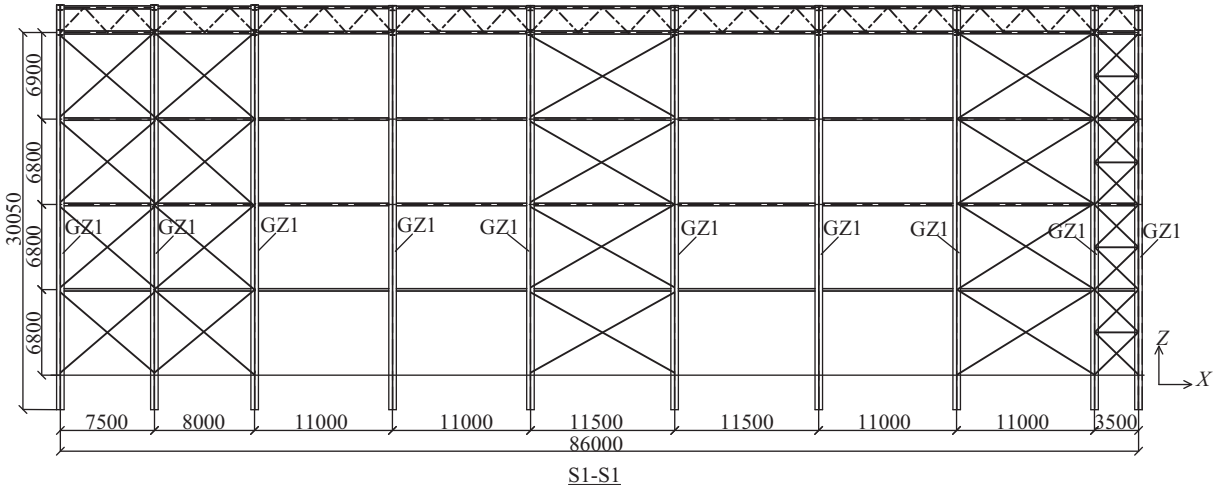

(c) Side view of the valve hall

Fig. 3. Diagram the ±800 kV UHV valve hall (unit: mm).

for external insulation. The configuration of the wall bushing and the facilities in the wall bushing are shown in Fig. 6.

Total length of the UHV wall bushing is 20.2 m, and the wall bushing weighs 11.45 t. Lengths of the indoor bushing, outdoor bushing and the metal connection part are 8.1 m, 10.1 m and 2.0 m, respectively. The wall bushing in the UHV converter substation is mounted on the gable wall of the valve hall with an inclined angle of 10°. Configuration and dimensions of the wall bushing mounted on the gable wall in the valve hall are shown in Fig. 5.

2.3. FE model and dynamic characteristics

The finite element software package ABAQUS [20] was adopted to simulate the wall bushing-valve hall system. In the FE model, the beams, columns and braces of the valve hall are simulated by B31 beam elements. Additionally, the installation plate in the valve hall for mounting the bushing is simulated by S4R shell elements. For the wall bushing, the C3D8R solid elements are used to simulate the polymer insulators, central conductor and flanges. In addition, some simplifications

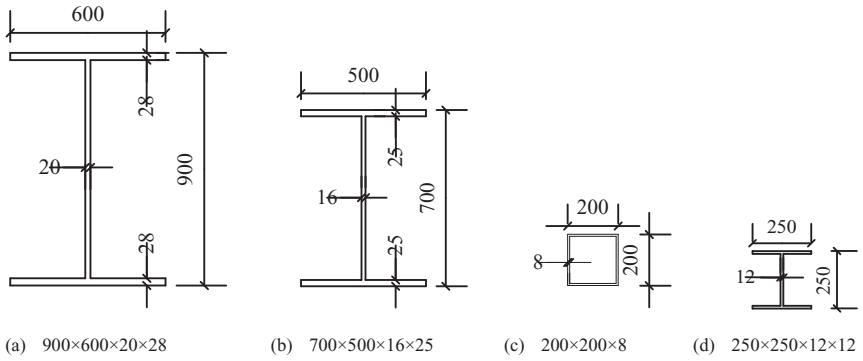

Fig. 4. Shapes and dimensions of cross sections of beams, columns and braces of the valve hall (unit: mm).

had to be made in the FE model, i.e., a) the silicon rubber sheds around the bushings for external insulation and the resin-impregnated paper capacitor packet around the central conductor for internal insulation were simplified as equivalent masses because Young's modulus of them were small; b) the equivalent density of the polymer insulators was increased to simulate the weight of the dielectric oil inside the UHV wall bushing and to maintain the location of the center of gravity without changing the dynamic characteristics of the UHV wall bushing; c) the connections of all components in the UHV wall bushing are rigid in the FE model. In the FE model of the wall bushing, the Young's modulus of 16 GPa and 70 GPa for the polymer material and the aluminum conductor, respectively, were provided by the manufacturer. After considering the assumptions listed above, the equivalent density of the polymer insulators and the conductors are 6040 kg/m^3 and 2417.8 kg/m^3.

The FE model and the coordinates of the UHV wall bushing-valve hall system is shown in Fig. 7. The *X*, *Y* axis and the *Z* axis are parallel and perpendicular to the horizontal plane, respectively. The wall bushing was mounted in a *Y*-*Z* vertical plane. According to the IEEE 693 standard and GB 50260 standard, damping ratios of each mode in the system were set at 2.0% [18,19]. The FE model of the wall bushing was also adopted in a simulation of shaking table tests and the wall bushing FE model was validated by the tests [17].

In mode analysis, the first resonance frequency of the whole system is 1.185 Hz, and the corresponding mode shape is the bending deformation of the busing in the *Y* direction. For the valve hall, the first resonance frequency is 2.152 Hz, which was the frequency of the lateral vibration of the structure (in the *Y* direction). In addition, the fundamental frequency of the UHV wall bushing mounted on the rigid base (without valve hall) is 1.51 Hz, which indicates that the steel valve hall would decrease the frequencies of the system. To simulate the rigid base, six degrees of freedom (DoFs) of the edge of the bottom plate of the flange of the wall bushing was constrained directly.

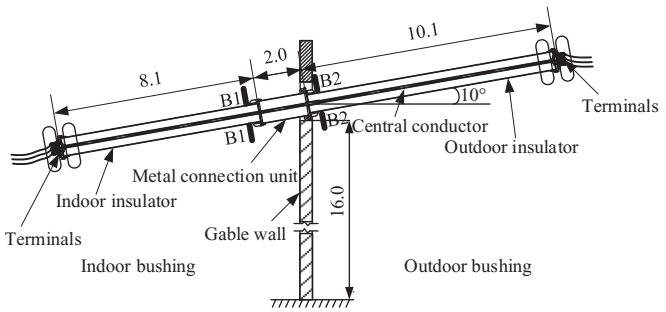

Fig. 5. Dimensions of the wall bushing (unit: m).

3. Seismic performance of UHV wall bushing-valve hall system

3.1. Earthquake ground motions

To evaluate the seismic performance of the wall bushing-valve hall system, 16 earthquake ground motions were selected from the Pacific Earthquake Engineering Research Center (PEER) ground motion database [21] and were modified by SeismoMatch software [22]. After that, the acceleration response spectrum (ARS) of the 16 earthquake ground motions could envelope the required response spectra (RRS) in the GB 50260 standard [18]. According to the standard [18], the ARS has a 2% exceedance probability in 100 years as shown in Fig. 8(a). The zero period acceleration (ZPA) in RRS should be 0.4 g in the main vibration direction and the ratios of the ZPA in different directions should be *Y*:*X*:*Z* = 1:0.85:0.65, which means that the ZPA in the *X* axis and *Z* axis are 0.34 g and 0.26 g, respectively. The coordinates for the 16 earthquake ground motions are same as the coordinates in Fig. 7. When the damping ratio is 2.0%, the ARS and the mean ARS of the 16 earthquake ground motions in different directions, compared with the RRS, are shown in Fig. 8. According to Fig. 8, the mean ARS of the 16 time histories could accommodate the RRS well. Peak ground acceleration (PGA) and other information of these 16 time histories are listed in Table 2.

3.2. Seismic responses of the system

In previous earthquakes, bushings and post insulators have always fractured at their base cross sections (Section B1-B1 and B2-B2 in Fig. 5), which means that the stress responses in the base cross sections of the indoor and outdoor insulators are critical parameters for evaluating the seismic performance of the wall bushing. The maximum stresses of the insulators of indoor and outdoor bushings were obtained under the excitation of time history RSN1504, and the corresponding values are 95.88 MPa and 87.53 MPa, respectively. With reference to the standard [18], the safety factor is defined as the ratio of ultimate strength of the polymer material to the maximum stresses in the insulators. Considering the ultimate strength of 75 MPa for the polymer material provided

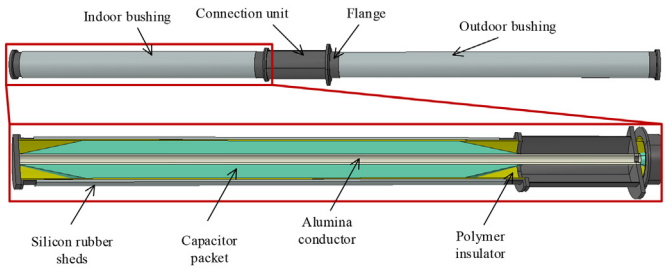

Fig. 6. Configuration of the UHV wall bushing, and the conductor and capacitor packet in the wall bushing.

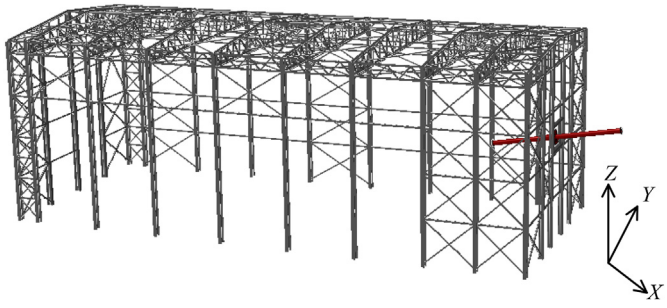

Fig. 7. FE model of UHV wall bushing-valve hall system.

by the manufacturer, safety factors of the wall bushing under excitation of RSN1504 are 0.78 and 0.86. Both of them are much less than 1.67, the recommended value in the standard [18]. Moreover, the safety factors of the indoor and outdoor insulators are less than 1.0, which means that the wall bushing will be destroyed in the corresponding earthquake. Considering the excitation of the 16 earthquake ground motions, the average maximum stress responses of the indoor and outdoor insulators are 73.16 MPa and 69.96 MPa, respectively, which means that the average safety factors are still less than 1.67 and the seismic performance of the wall bushing-valve hall system should be improved.

To evaluate the dynamic interaction between the valve hall and the wall bushing, the seismic responses of the wall bushing mounted on a rigid base were analyzed for a comparison. The 16 earthquake ground motions were input at the base of the wall bushing and the average maximum stress in the base cross sections of the indoor and outdoor insulators are 26.00 MPa and 24.14 MPa, respectively, which means that the safety factors are 2.88 and 3.11, respectively, which is larger than 1.67. These factors satisfy the requirements in the GB 50260 standard [18]. The stress amplification factor (SAF) is defined as the ratio of the maximum stresses of wall bushing mounted on the valve hall under each earthquake ground motion to those of the wall bushing mounted on a rigid base under the corresponding earthquake ground motion. Comparing the wall bushing mounted on the wall of the valve hall and rigid base, the average SAFs of the indoor and outdoor insulators under the 16 earthquake ground motions are 2.84 and 2.95, which means that the stress responses of the wall bushing are amplified by the steel valve hall.

According to the stipulations in the IEEE 693 standard [19] and the GB 50260 standard [18], to evaluate the seismic performance of electric equipment, the equipment should be tested by mounted on a rigid adapter and the amplification factor of the support should be considered in the input of the test. An appropriate dynamic amplification factor simulating the amplification effects of the valve hall should be adopted to evaluate the seismic performance of the wall bushing mounted on a rigid base. According to the average SAFs, the amplification factor could be set at 3 for a ± 800 kV UHV wall bushing.

Table 2
Information on the 16 modified earthquake ground motions.

Record no.	Earthquake name	Station	Year	Magnitude	Original PGA/g	Modified PGA/g
RSN6	Imperial Valley	El Centro	1940	6.95	0.23	0.41
RSN15	Kern County	Taft	1952	7.36	0.16	0.50
RSN125	Friul	Tolmezzo	1976	6.5	0.32	0.48
RSN139	Tabas	Dayhook	1978	7.35	0.33	0.45
RSN639	Whittier Narrows	Obregon	1987	5.99	0.41	0.63
RSN848	Landers	Coolwater	1992	7.28	0.35	0.36
RSN1045	Northridge	Newhall	1994	6.69	0.36	0.61
RSN1101	Kobe	Amagasaki	1995	6.9	0.31	0.48
RSN1158	Kocaeli	Duzce	1999	7.51	0.32	0.55
RSN1504	Chi-Chi	TCU067	1999	7.62	0.42	0.53
RSN1787	Hector Mine	Hector	1999	7.13	0.31	0.47
RSN3548	Loma Prieta	Los Gatos	1989	6.93	0.44	0.50
RSN3965	Tottori	TTR008	2000	6.61	0.39	0.58
RSN4031	San Simeon	Templeton	2003	6.52	0.43	0.55
RSN4800	Wenchuan	Zengjia	2008	7.9	0.42	0.39
RSN4896	Chuetsu-oki	Kashiwazaki	2007	6.8	0.39	0.45

Flexible bundled conductors are connected in the two terminals of the wall bushings to transmit electric current (Fig. 5). Many researchers found that the tensile force in conductors is one of the main reasons for the failure of electrical equipment in earthquakes when the seismic displacement of equipment was too large [23]. Average maximum displacements of the terminals of the indoor and outdoor bushings in the system are 298.12 mm and 238.47 mm, respectively. Necessary slackness should be allowed in the conductors to avoid the impact forces from conductors. Average displacements of the wall bushing terminals mounted on rigid base are 95.17 mm and 104.91 mm, respectively. After the wall bushing is mounted on the valve hall, the terminal displacements are almost doubled and can even triple the corresponding values of the wall bushing mounted on a rigid base.

4. Seismic interaction between wall bushing and valve hall

4.1. ARS of the wall bushing-valve hall system

Under the excitation of the 16 different earthquake ground motions, the average ARS at the terminals of the indoor bushing and outdoor bushing are shown in Fig. 9(a) and (b). The first two predominant frequencies of the ARS at the terminals of the indoor and outdoor bushing are 1.185 Hz and 2.15 Hz. The former one is the first resonance frequency of the wall bushing-valve hall system and the latter one is close to the first frequency of 2.152 Hz, which pertains to the valve hall itself. The peak value of the latter one, however, is much larger than the peak value of the ARS at 1.185 Hz. The prominent vibration frequency of the bushing is correlated with the resonance frequency of the valve hall, which indicates that the dynamic properties of the valve hall

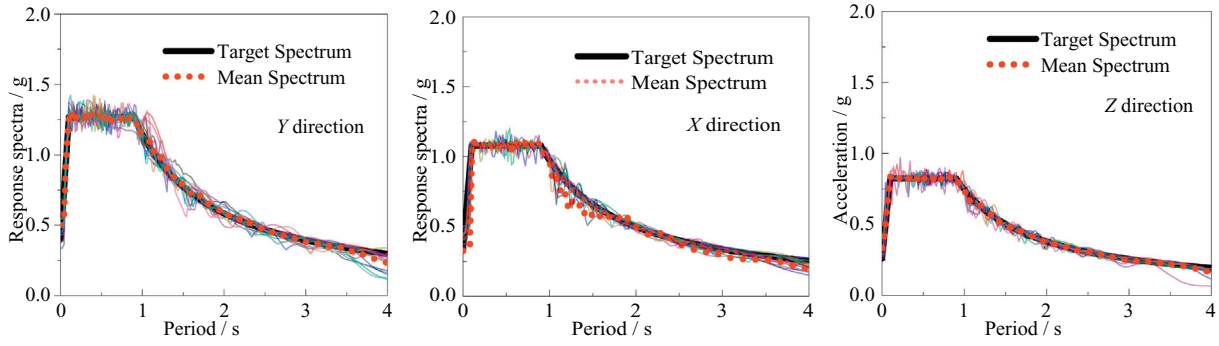

Fig. 8. RRS in Chinese standard and the mean spectra of the 16 earthquake time histories (damping ratio ξ = 0.02).

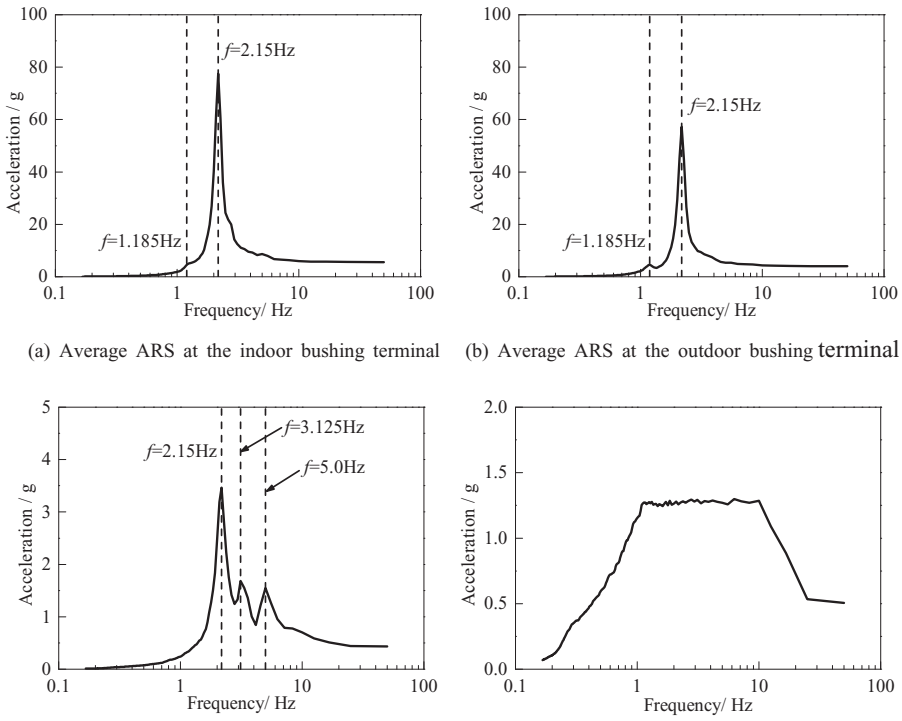

(a) Average ARS at the indoor bushing terminal (b) Average ARS at the outdoor bushing terminal

(c) Average ARS at the wall bushing base (d) Average ARS of 16 earthquake ground motions

Fig. 9. Average ARS at different positions of the wall bushing and the average ARS of the 16 earthquake ground motions (damping ratio $\xi = 0.02$).

has a great influence on the seismic responses of the wall bushing mounted on it. Moreover, in the ARS of the terminals of the indoor and outdoor bushing, there is no peak with the corresponding frequency of 1.51 Hz, which is the fundamental frequency of the wall bushing itself.

The average ARS at the base of the wall bushing and the average ARS of 16 earthquake ground motions in the *Y* direction are shown in Fig. 9(c) and (d), respectively. Comparing the two figures, the spectral characteristics at the base of the wall bushing are quite different from the input earthquake motions. The acceleration time histories at the base of the UHV wall bushing were filtered by the valve hall. Three predominant frequency points, 2.15 Hz, 3.125 Hz and 5.0 Hz, appeared in the ARS at the base of the wall bushing (Fig. 9(c)). Three mode shapes of the gable wall with similar resonance frequencies are shown in Fig. 10, and the corresponding frequencies of the three modes are 2.152 Hz, 3.131 Hz and 5.045 Hz, which are close to the predominant frequencies in Fig. 9(c). Fig. 10(a) and (b) represent the lateral and torsional vibration of the valve hall, respectively. In these two mode shapes, the vibration modes of the gable wall are similar and it vibrates in the *Y* direction. In Fig. 10(c), the out-of-plane rocking vibration mode of the gable wall is observed and the rocking effect also has an influence on the acceleration responses of the wall bushing, which is demonstrated by the third peaks in the ARS in Fig. 9(c). The differences between the three predominant frequencies in Fig. 9(c) and the three resonance frequencies of the mode shapes in Fig. 10 are influenced by the mass of the wall bushing.

4.2. Vibration components of wall bushing

To analyze the interaction between the wall bushing and the valve hall, a simplified theoretical model of the system was established (Fig. 11(a)). The indoor and outdoor bushings were simplified as cantilever beams and the constraints of the valve hall were abstracted to springs to support the bushing. L_i and L_o denote the length of the indoor and outdoor bushings, respectively, and a denotes the diameter of the flange plate of the metal connection unit of the wall bushing.

Taking the horizontal deformation of the outdoor bushing as an example, the seismic displacements of the bushing could be decomposed into three parts (Fig. 11(b)). The total terminal displacements D of the outdoor bushing is

$$D = d_1 + d_2 + d_3 \tag{1}$$

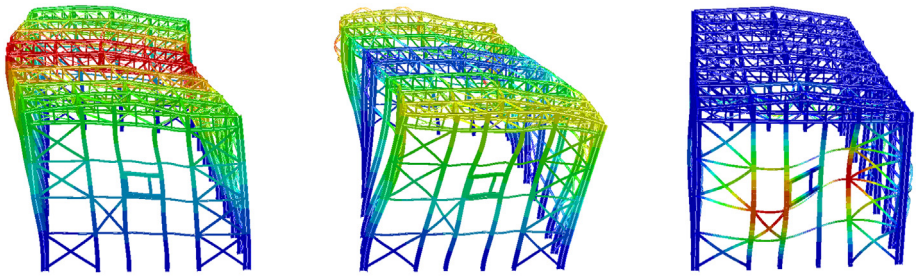

(a) Lateral vibration at 2.152 Hz (b) Torsion vibration at 3.131 Hz (c) Out-of-plane rocking at 5.045Hz

Fig. 10. Three mode shapes and corresponding frequencies of the gable wall.

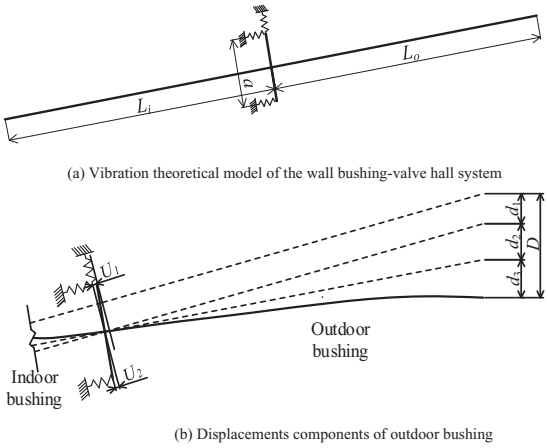

Fig. 11. Vibration theoretical model and displacement decomposition of the UHV wall bushing-valve hall system.

where d_1 is the translational displacement generated by the deformation of the valve hall. d_2 is the rotational displacement from the rocking effect of the gable wall. d_3 is the deformation of the bushing itself. θ denotes the out-of-plane rotational angle of the gable wall. The displacements perpendicular to the flange plate at the left and the right side edges of the flange at the base of the connection unit are represented by U_1 and U_2 (Fig. 11(b)). d_2 and θ could be represented by Eqs. (2) and (3).

$$d_2 = \theta L_o \tag{2}$$

$$\theta = \frac{U_1 - U_2}{a} \tag{3}$$

Substituting Eqs. (2) and (3) into Eq. (1), the acceleration components can be obtained by finding the second derivative of Eqs. (1) and (3):

$$A = A_t + A_r + A_b \tag{4}$$

$$A_r = \frac{A_1 - A_2}{a} L_o \tag{5}$$

In Eqs. (4) and (5), A denotes the total acceleration of the wall bushing. A_1 and A_2 are the accelerations obtained at the left and the right side edge of the metal flange, corresponding to U_1 and U_2. A_r denotes the acceleration generated by the rocking effect. A_t is the horizontal acceleration in the Y direction at the base of the bushing as well as the translational acceleration generated by displacements of the valve hall, and A_b is the acceleration generated by bushing deformation. In Eqs. (4) and (5), A_t, A_1, A_2 and A could be obtained from the FE results. Moreover, a equals 1320 mm, and L_o equals 10.1 m in this UHV wall bushing.

Taking the seismic responses of the outdoor bushing under the excitation of earthquake RSN6 as an example, A, A_r and A_t were obtained from the FE results and A_b could be calculated according to Eq. (4). The acceleration components are shown in Fig. 12. Comparing the four figures, the acceleration generated by the bending deformation contributes to a large proportion of the total terminal acceleration, followed by the acceleration generated by the translational vibration from the deformation of the valve hall.

4.3. Moment components at the base cross section of bushing

It is assumed that the mass of the wall bushing is m, and the mass is evenly distributed over the length of the wall bushing. The moment M_t at the base cross section is generated by translation component A_t and

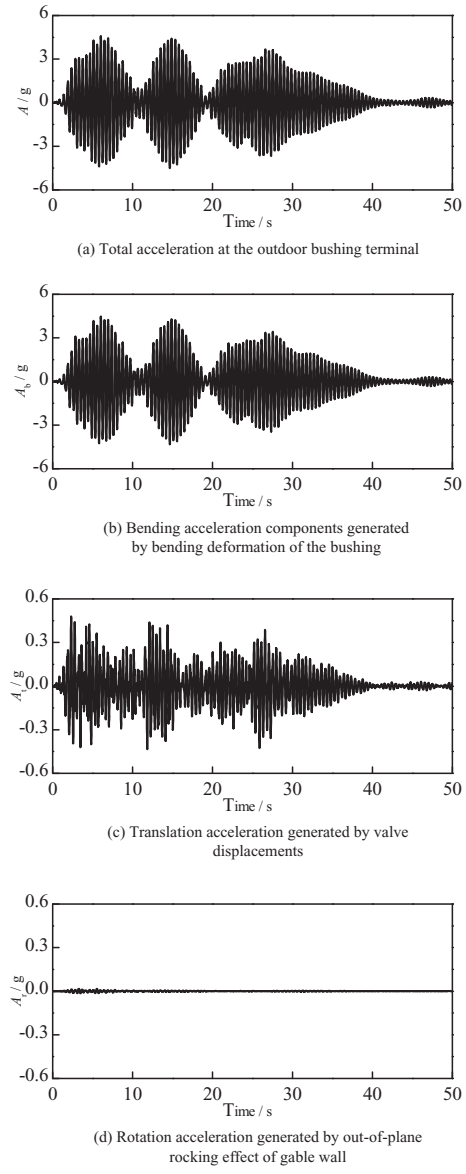

Fig. 12. Total acceleration and different acceleration components at the terminal of outdoor bushing.

the moment M_r, generated by rocking component A_r, can be represented by Eqs. (6) and (7), respectively. The moment M_t and moment M_r can be expressed as

$$M_t(t) = mA_t(L_o, t)\frac{L_o}{2} \tag{6}$$

$$M_r = J\alpha(t) = \frac{1}{3}mL_oA_r(L_o, t) \tag{7}$$

where t, J and α denote time, the rotational inertia of the outdoor bushing and the angular acceleration of the gable wall, respectively. For the bending deformation of the outdoor bushing itself, the deformation could be assumed as Eq. (8) [24], which is expressed as

$$d_3(x, t) = \Phi(x)D_t(t) \tag{8}$$

where Φ is the deformation mode shape matrix of the outdoor bushing mounted on a rigid base, and D_t is the amplitude time history matrix of the terminal displacements generated by different mode shapes. The

displacement of the bushing-like electrical equipment is mainly attributed to the first vibration mode [23]. The bending mode of the outdoor bushing in the theoretical model is assumed as the first mode shape of a cantilever beam without loss of generality as shown in Eq. (9) [24].

$$\Phi(x) = \cos(ax) - \cosh(ax) - \frac{\cos(aL_o) + \cosh(aL_o)}{\sin(aL_o) + \sinh(aL_o)}(\sin(ax) - \sinh(ax)) \tag{9}$$

where $aL_o = 1.875$. The amplitude D_t and second derivative $\ddot{D}_t$ can be obtained by Eq. (10).

$$\begin{cases} D_t(t) = \dfrac{d_3(L_o,t)}{\Phi(L_o)} \\ \ddot{D}_t(t) = \dfrac{\ddot{d}_3(L_o,t)}{\Phi(L_o)} \end{cases} \tag{10}$$

And, the moment at the base cross section generated by the bending deformation can be obtained according to Eq. (11).

$$M_b(t) = \frac{m}{L_o}\int_0^{L_o} A_b(L_o,t)x\frac{\Phi(x)}{\Phi(L_o)}dx \tag{11}$$

where

$$A_b(x,t) = \Phi(x)\ddot{D}(t) = \ddot{d}_3(L_o,t)\frac{\Phi(x)}{\Phi(L_o)} = A_b(L_o,t)\frac{\Phi(x)}{\Phi(L_o)} \tag{12}$$

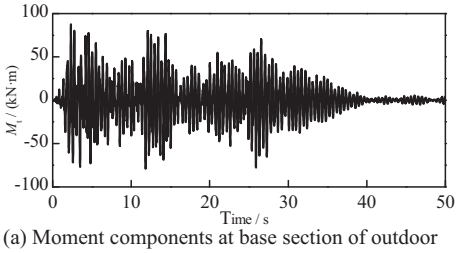

(a) Moment components at base section of outdoor bushing generated by translation displacements of valve hall

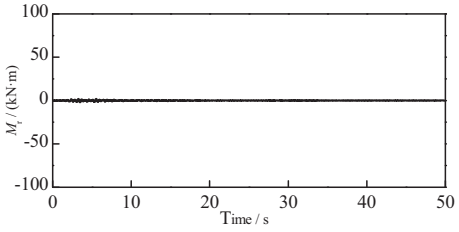

(b) Moment components at base section of outdoor bushing generated by rotational displacements of out-of-plane rocking effect of gable wall

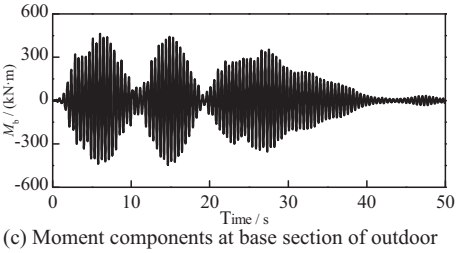

(c) Moment components at base section of outdoor bushing generated by bending deformation of outdoor bushing itself

Fig. 13. Moment components at base section of outdoor bushing generated by different vibration components.

Different moment components at the base cross section of the outdoor bushing can be obtained by Eqs. (6), (7) and (11) (Fig. 13). According to Fig. 13(a) and (b), the peak moment generated by translation is 44.57 times that of the peak moment generated by the out-of-plane rocking vibration of the gable wall of the valve hall. Comparing Fig. 13 (a) and (c), the peak moment generated by translation is 18.9% of the peak moment in Fig. 13(c), generated by the bending deformation of the outdoor bushing itself. The translation component generates a large moment at the base section of the wall bushing.

5. Measures for improving seismic performance of the system

5.1. Retrofitting measures

According to the analysis above, the displacements of the valve hall would generate moments (translation component) at the base cross sections of the wall bushing, which means that increasing the lateral (Y direction) stiffness of the gable wall to suppress the translational

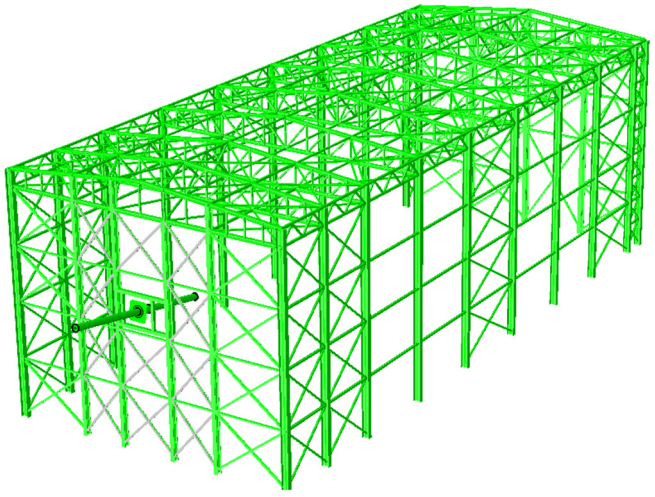

(a) Retrofit of countermeasure Type I for valve hall

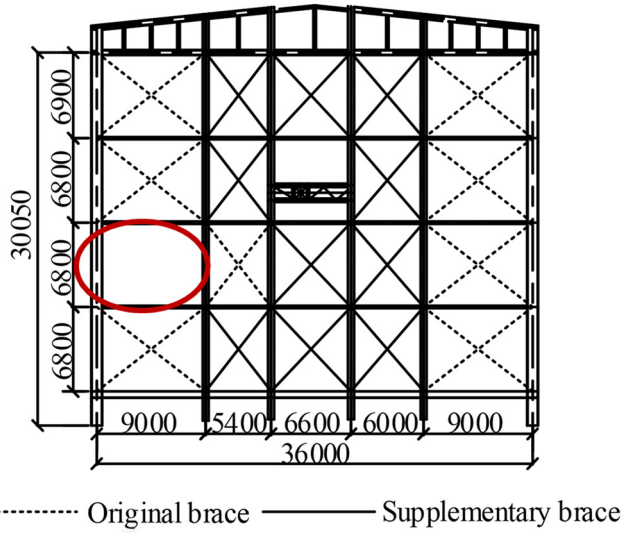

(b) Sketch diagram of original and supplementary braces in gable wall (Unit: mm)

Fig. 14. Retrofit countermeasure Type I for the valve hall.

component could decrease the seismic responses of the wall bushing. To increase the stiffness of the gable wall of the valve hall, two measures were carried out and verified in the FE model.

Many UHV electric facilities, e.g., thyristor valves and post insulators, are installed in the valve hall and the DC yard. In order to keep the electrical clearance between the equipment and metal structures, the retrofitting measures cannot be set in the valve hall and the DC yard. Type I retrofit measure is defined as adding supplementary braces in the gable wall (Fig. 14(a)). The cross section of the supplementary braces is in an H shape and the dimensions are 250× 250 × 12 × 12, which is the same dimensions as the cross sections of the original braces. The arrangement of the original and supplementary braces can be found in Fig. 14(b). In the circle of Fig. 14(b), a ±400 kV wall bushing should be installed, so there is no brace in this position. In order to further increase the lateral stiffness of the gable wall, the concrete shear wall was assembled in the model and the retrofitting measure was referred to as Type II (Fig. 15). The thickness of the concrete shear wall is 400 mm and the type of concrete is C30, which is a common concrete type in China [25].

In the FE model, the supplementary braces and concrete shear wall are simulated by the B31 beam element and S4R shell element in Abaqus software [20], respectively. The steel braces and the concrete shear walls do not occupy the room in the valve hall and the converter station, and do not affect the electrical clearance between the equipment and the structure, so they meets the electrical requirements. Moreover, comparing to the cost of damping and insulation measures, the two retrofit measures is cheap. And they are convenient to be taken in the projects under construction or completed projects.

5.2. Dynamic properties of retrofitted system

The sequence number of the modes and the corresponding frequencies of the lateral or out-of-plane rocking vibration of the gable wall after retrofitting are listed in Table 3. After the valve hall was retrofitted, the frequencies of the vibration increased. The maximum displacements of the gable wall in the corresponding mode shape are also listed in Table 3, and the deformation amplitude of the gable wall was much less than that before retrofitting. According to the analyses above, the lateral vibration model shape of the gable wall has great influence on the seismic responses of the wall bushing. According to Table 3, in the original structure of the valve hall, the gable wall, vibrated in the first mode shape. After retrofitted by retrofit countermeasure Type I, the main deformation in this mode shape is at the middle region of the valve hall (Fig. 16(a)). In the valve hall of retrofit countermeasure Type II, the out-of-plane rocking accompanied by a small amount of lateral vibration could be observed in the gable wall (Fig. 16(b)). As Fig. 9(c) shows, both deformation types influenced the acceleration input at the base of the UHV wall bushing.

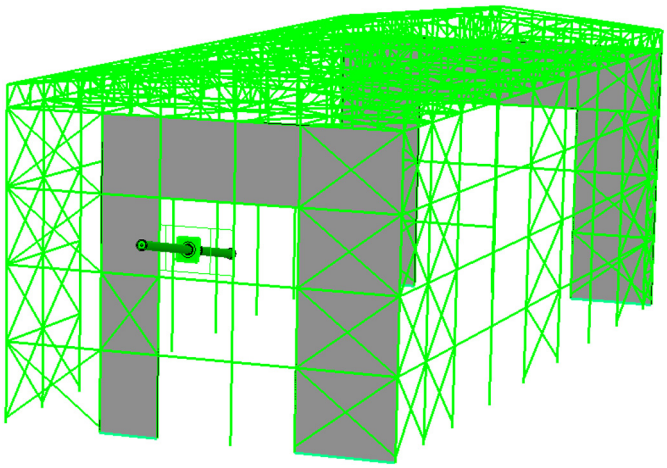

Fig. 15. Retrofit countermeasure Type II for valve hall.

5.3. Retrofitting effects analysis

To evaluate the seismic performance of the retrofitted wall bushing-valve hall system, the seismic responses of the system are analyzed using the earthquake ground motions listed in Table 2. The peak stresses at the base cross sections of the indoor and outdoor insulators under the 16 earthquake ground motions before and after retrofitting are shown in Fig. 17. According to Fig. 17, the average maximum stresses after retrofitting are much less than the responses of the original structure. For retrofit countermeasure Type I, the maximum stresses of the indoor and outdoor insulators are 44.53 MPa and 41.44 MPa, much less than the maximum stresses before retrofitting. The safety factors of the two insulators are 1.68 and 1.81. For retrofit countermeasure Type II, the maximum stresses are 43.75 MPa and 44.77 MPa, which means the safety factors are 1.71 and 1.68 for indoor and outdoor insulators, respectively. The safety factors are all larger than 1.67, recommended by standard GB 50260 [18], which means that the seismic performance of the system after retrofitting meets the requirements in the corresponding standard [18]. Considering the stress responses of the wall bushing mounted on a rigid base, the SAFs of the valve hall after retrofitting could be set at 2. Moreover, the safety factors of the retrofitted system are close to the limited value.

The peak terminal displacements of the indoor and outdoor bushings under the exact measurements of different earthquake ground motions before and after retrofitting are shown in Fig. 18. In terms of the maximum terminal displacements, the average peak values after retrofitting by the two measures are about half the corresponding value of the structure before it was retrofitted. After retrofitting, the wall bushing is more convenient for the design of coupling facilities, e.g. flexible bundled conductors. In conclusion, the retrofitting measures could improve the seismic performance of the wall bushing-valve hall system.

The ARS at the base of the wall bushing in the *Y* direction of the original and retrofitted structures are shown in Fig. 19(a). In the ARS, the first predominant frequency of each ARS at the base of the wall bushing are 2.15 Hz, 2.63 Hz and 2.94 Hz, respectively, which is similar to the natural frequencies of the valve hall before and after retrofitting (Table 3). After retrofitting, the peak value of the response spectra decreased and the increase of the predominant frequencies in the spectrum could be observed. The ARS peak values of the retrofitted structure are much less than the corresponding values of the original structure, which are in accordance with the tendency of the stress and displacement responses before and after retrofitting. Moreover, this ARS declination is the first reason for the reduction of seismic responses. The differences between the predominant frequencies of the ARS and the fundamental frequency of the bushing itself are enlarged, which is the second reason for the reduction of the seismic responses. This phenomenon is in accordance with the conclusion in reference [14].

Table 3
Mode number, frequency, and the vibration mode of the valve hall after retrofitting.

Retrofit no.	Mode no.	Frequency/Hz	Displacements of gable wall in mode shape	Mode shape
Origin	1st	2.15	0.26	Lateral vibration
Type I	5th	2.63	0.0019	Lateral vibration
Type II	12th	2.94	0.0017	Out-of-plane rocking with lateral vibration

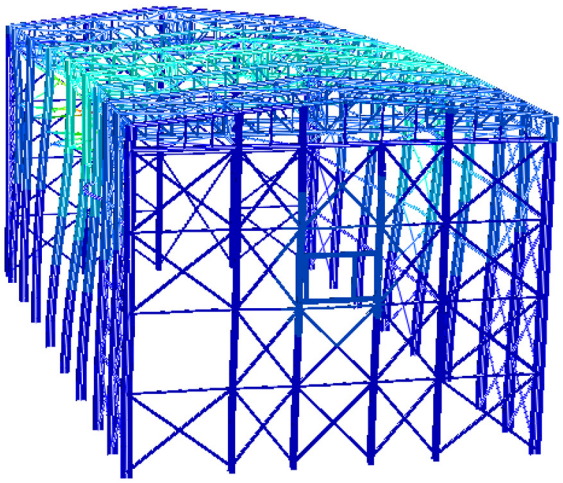

(a) First mode shape of the gable wall of Type I retrofit measure

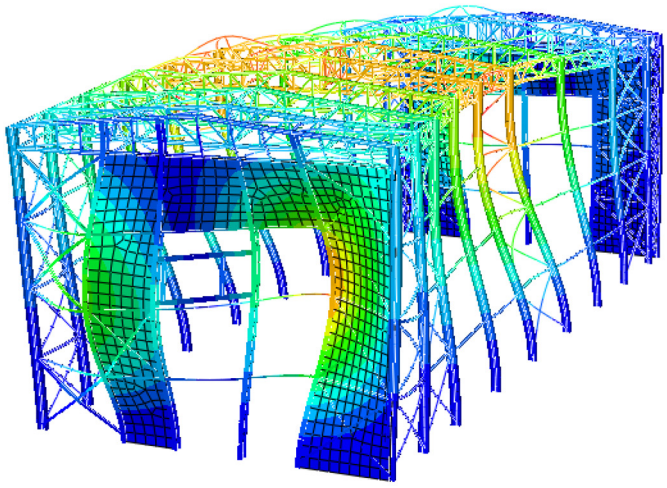

(b) 12th mode shape of the gable wall of Type II retrofit measure

Fig. 16. Mode shapes of the gable wall after retrofitted.

The ARS in the *Y* direction at the terminals of the indoor and outdoor bushings in the original structure and the two retrofitted structures are shown in Fig. 19(b) and Fig. 19(c). The peak values of the retrofitted UHV wall bushing-valve hall system decreased. This means that increasing the lateral stiffness of the gable wall by braces or by a concrete shear wall could improve the seismic performance of the wall bushing-valve hall system.

In Fig. 19(a), the second peak value of Type II retrofit measure is larger than others and the corresponding frequency of the peak is 4.94 Hz. The 53rd mode shape of the valve hall with Type II retrofit measure, of which the frequency is 4.941 Hz, is shown in Fig. 20. The wall bushing is mounted on the frame in the gable wall (shown in the circle in Fig. 20). In the 53rd mode shape, the displacement of the mounting frame is 1.0, which is the maximum value in model shape. The displacements of the frame in other mode shapes or in Type I retrofit measure are listed in Table 3 in the revised manuscript, and they are less 1. This is the reason why the second peak of the acceleration response spectra of Type II retrofit measure is greater than others.

6. Conclusions

The results of the numerical study on a ±800 kV UHV wall bushing-valve hall system indicate that the seismic performance of the system cannot meet the requirements in the Chinese GB 50260 standard. The strength safety factors of both indoor and outdoor polymer insulators are less than the recommended value in the standard. The valve hall has an amplification effect on the seismic responses of the wall bushing. Stress amplification factor is close to 3 as the wall bushing is mounted on the valve hall. When evaluating the seismic performance of a wall bushing mounted on a rigid base, the dynamic amplification effect of the valve hall cannot be ignored and a dynamic amplification factor should be taken into consideration.

The translational component generated by the vibration of the valve hall ranks only second to the vibration component generated by the bending of the bushing itself. Increasing the lateral stiffness of the gable wall could restrain the vibration of it and reduce the seismic responses of the wall bushing. The peaks of the acceleration response spectra at the base of the wall bushing reduced, and the predominant frequencies of the response spectra increased, which decreased the amplification effect of the valve hall and the seismic responses of the UHV wall bushing.

The lateral stiffness of the gable wall could be increased by supplementary braces or concrete shear wall. After increasing the lateral stiffness of the gable wall, the seismic performance of the system will be improved. Under the excitation of the precautionary earthquake ground motions and after retrofitting by the two types of measures, the average safety factors are larger than the recommended value in the Chinese standard [18].

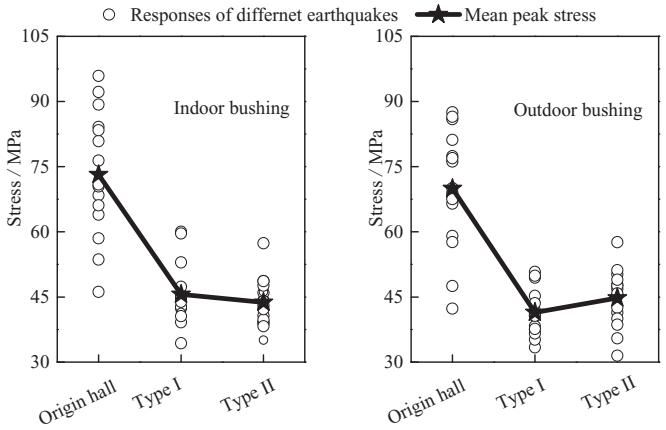

Fig. 17. Maximum stress responses at the wall bushing base sections before and after retrofitting.

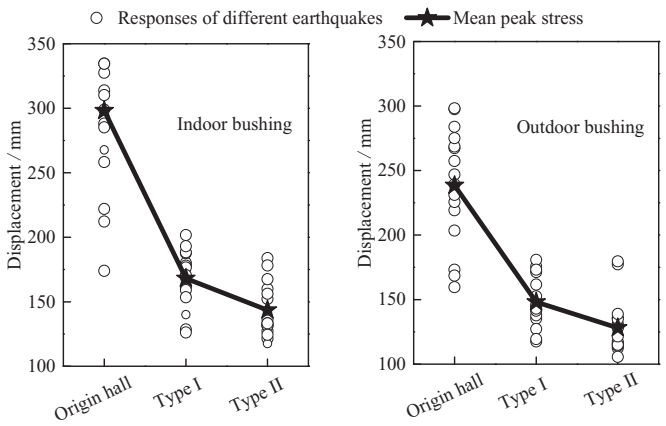

Fig. 18. Maximum tip displacements responses of a wall bushing before and after retrofitted.

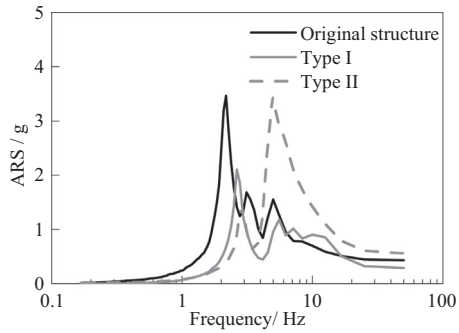

(a) The ARS of the original and two retrofitted structures at the base of the wall bushing

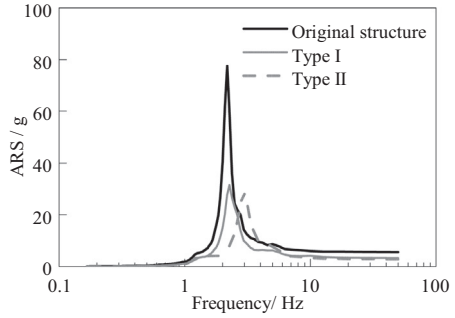

(b) The ARS of the original and two retrofitted structures at the terminal of the indoor bushing

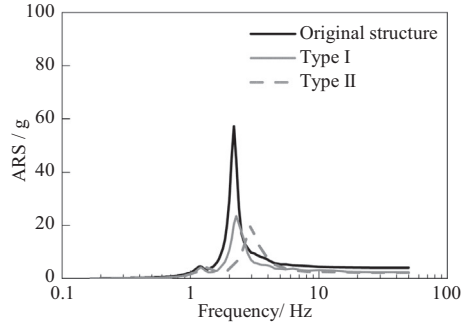

(c) The ARS of the original and two retrofitted structures at the terminal of the outdoor bushing

Fig. 19. The ARS of the original and two retrofitted structures at different positions.

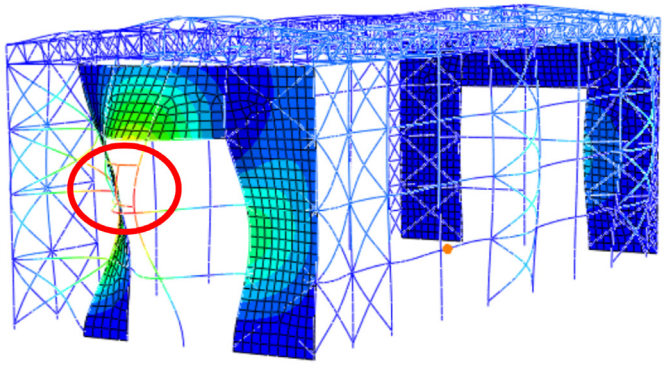

Fig. 20. The 53rd mode shape of the valve hall with Type II retrofit measure.

The stiffness of the valve hall would affect the seismic performance of the wall bushing mounted on it. Further investigation needs to be carried out on the relationship between the stiffness of the valve hall and the seismic performance of the wall bushing. As increasing the stiffness of the valve hall could decrease the seismic responses of the wall bushing, after further investigation, the minimum stiffness ratio of the valve hall to the wall bushing needs to be put forward.

Acknowledgements

This study was financially supported by the National Key R&D Program of China (Grant No. 2018YFC0809400) and the National Natural Science Foundation of China (Grant No. 51878508). Their support is greatly appreciated.

References

[1] A.J. Schiff, Guide to Improved Earthquake Performance of Electric Power Systems, US Department of Commerce, National Institute of Standards and Technology, 1998.
[2] A.J. Schiff, Northridge Earthquake: Lifeline Performance and Post-Earthquake Response, ASCE, 1995.
[3] T. Mishima, T. Yokomura, A. Takahashi, Lessons learned from the transformer fire in the Niigata-ken Chuetsu-oki Earthquake and actions for solving the problems, Fire Disaster 58 (2) (2008) 5–10 (in Japanese).
[4] Q. Xie, R. Zhu, Damage to electric power grid infrastructure caused by natural disasters in China, IEEE Power Energy Mag. 9 (2) (2011) 28–36.
[5] Tokyo Electric Power Co. Ltd, Power Failure Recovery Record of Electrical Equipment Due to Tohoku Region Pacific Offshore Earthquake. Tokyo, Japan, http://www.tepco.co.jp/torikumi/thermal/images/teiden_hukkyuu.pdf 2013 (in Japanese).
[6] A. Kwasinski, J. Eidinger, A. Tang, Performance of electric power systems in the 2010-2011 Christchurch, New Zealand, earthquake sequence, Earthq. Spectra 30 (1) (2014) 205–230.
[7] D. Huang, Y. Shu, J. Ruan, Y. Hu, Ultra high voltage transmission in China: developments, current status and future prospects, Proc. IEEE 97 (3) (2009) 555–583.
[8] Y. Shu, W. Chen, Research and application of UHV power transmission in China, High Volt. 3 (1) (2018) 1–13.
[9] S. Ersoy, S. Feizi, A. Ashrafi, M.A. Saadeghvaziri, Seismic Evaluation and Rehabilitation of Critical Components of Electrical Power Systems, 2006, Buffalo, New York.
[10] M. Koliou, A. Filiatrault, A.M. Reinhorn, Seismic response of high-voltage transformer-bushing systems incorporating flexural stiffeners I: Numerical study, Earthquake Spectra 29 (4) (2013) 1335–1352.
[11] A. Filiatrault, H. Matt, Seismic response of high voltage electrical transformer - bushing systems, J. Struct. Eng. 132 (2) (2006) 287–295.
[12] M. Koliou, A. Filiatrault, A.M. Reinhorn, Seismic response of high-voltage transformer-bushing systems incorporating flexural stiffeners II: experimental study, Earthquake Spectra 29 (4) (2013) 1353–1367.
[13] R.K. Mohammadi, V. Akrami, F. Nikfar, Dynamic properties of substation support structures, J. Constr. Steel Res. 78 (2012) 173–182.
[14] S. Günay, K.M. Mosalam, Seismic performance evaluation of high-voltage disconnect switches using real-time hybrid simulation: II. Parametric study, Earthq. Eng. Struct. Dyn. 43 (8) (2014) 1223–1237.
[15] S. Li, H. Tsang, Y. Cheng, Z. Lu, Considering seismic interaction effects in designing steel supporting structure for surge arrester, J. Constr. Steel Res. 132 (2017) 151–163.
[16] A.S. Whittaker, G.L. Fenves, A.S.J. Gilani, Seismic evaluation and analysis of high-voltage substation disconnect switches, Eng. Struct. 29 (12) (2007) 3538–3549.
[17] Q. Xie, C. He, Y. Zhou, Seismic evaluation of ultra-high voltage wall bushing, Earthq. Spectra (2018) (in press).
[18] GB 50260, Code for Seismic Design of Electrical Installations, Beijing, 2013 (in Chinese).
[19] IEEE Standard 693, IEEE Recommended Practice for Seismic Design of Substations, New York, 2005.
[20] Cooperation Dassault Simulia, Abaqus/CAE User's Manual (Version 6.10). USA, 2010.
[21] Pacific Earthquake Engineering Research Center, PEER Ground Motion Database, 2011.
[22] Seismosoft, SeismoMatch v2.1 - A Computer Program for Spectrum Matching of Earthquake Records. USA, 2013.
[23] J.B. Dastous, A. Filiatrault, J. Pierre, J, Estimation of displacement at interconnection points of substation equipment subjected to earthquakes, IEEE Trans. Power Deliv. 19 (2) (2004) 618–628.
[24] R.W. Clough, J. Penzien, Dynamics of Structures, 2nd ed. McGraw-Hill Publishing Company, New York, 1993.
[25] GB 50010-2010, Code for Design of Concrete Structures, Beijing, 2010 (in Chinese).